On the effects of improved cross-section representation in one-dimensional flow routing models applied to ephemeral rivers

Christopher J. Hutton,[1,2] Richard E. Brazier,[2] Andrew P. Nicholas,[2] and Mark Nearing[3]

Received 18 August 2011; revised 2 March 2012; accepted 3 March 2012; published 10 April 2012.

[1] Flash floods are an important component of the semiarid hydrological cycle, and provide the potential for groundwater recharge as well as posing a dangerous natural hazard. A number of catchment models have been applied to flash flood prediction; however, in general they perform poorly. This study has investigated whether the incorporation of light detection and ranging (lidar) derived data into the structure of a 1-D flow routing model can improve the prediction of flash floods in ephemeral channels. Two versions of this model, one based on an existing trapezoidal representation of cross-section morphology (K-Tr), and one that uses lidar data (K-Li) were applied to 5 discrete runoff events measured at two locations on the main channel of The Walnut Gulch Experimental Watershed, United States. In general, K-Li showed improved performance in comparison to K-Tr, both when each model was calibrated to individual events and during an evaluation phase when the models (and parameter sets) were applied across events. Sensitivity analysis identified that the K-Li model also had more consistency in behavioral parameter sets across runoff events. In contrast, parameter interaction within K-Tr resulted in poorly constrained behavioral parameter sets across the multidimensional parameter space. These results, revealed with a modeling focus on the structure of a particular element of a distributed catchment model, suggest that lidar derived cross-section morphology can lead to improved, and more robust flash flood prediction.

Citation: Hutton, C. J., R. E. Brazier, A. P. Nicholas, and M. Nearing (2012), On the effects of improved cross-section representation in one-dimensional flow routing models applied to ephemeral rivers, *Water Resour. Res.*, *48*, W04509, doi:10.1029/2011WR011298.

1. Introduction

[2] Flash floods are defined as runoff events that occur within 6 hours of the causative rainfall event [*National Weather Service*, 2002], and are the dominant runoff response in many ephemeral semiarid catchment systems [*Goodrich et al.*, 1997; *Garcia-Pintado et al.*, 2009]. Flash floods are important elements of the semiarid hydrological cycle that must be understood for two primary reasons. First, these intermittent events provide potential for groundwater recharge via transmission losses (e.g., infiltration through the streambed), and are therefore an important water resource in semiarid environments [*Coes and Pool*, 2005; *Morin et al.*, 2006]. Second, flash floods present a dangerous natural hazard that can detrimentally impact channel morphology [*Hooke and Mant*, 2000], human infrastructure [*Foody et al.*, 2004], and cause a significant number of fatalities [*Ashley and Ashley*, 2008].

[3] A number of models have been developed to predict and understand semiarid catchment hydrology, including: empirical regression-based models [*McIntyre et al.*, 2007]; semiempirical models [*McIntyre and Al-Qurashi*, 2009]; spatially lumped models (e.g., Sacramento Soil Moisture Accounting Model [*Burnash*, 1995]); and distributed process based models [*El-Hames and Richards*, 1998], including the Kinematic Runoff and Erosion model (KINEROS) [*Smith et al.*, 1995].

[4] The development of distributed process based models has attempted to overcome some of the empirical limitations of simpler model structures. However, predictions derived from distributed process based models are highly uncertain owing to uncertain parameter values and boundary conditions [*Yatheendradas et al.*, 2008; *Garcia-Pintado et al.*, 2009], and because of epistemic uncertainty surrounding the processes themselves. A significant source of model uncertainty results from a paucity of spatial information, notably information on distributed rainfall and hillslope infiltration properties [*Al-Qurashi et al.*, 2008; *Yatheendradas et al.*, 2008]. In data poor situations, predictions derived from simpler (semi-) empirical models may be preferred, and indeed may be less uncertain [*McIntyre et al.*, 2007; *McIntyre and Al-Qurashi*, 2009]. Simpler models, however, may not be appropriate to resolve adequately key temporal and spatial processes controlling flash flooding in semiarid environments. Simulation of these processes is required to understand and resolve the complex processes, thresholds and interactions that govern the rainfall-runoff response in different semiarid catchments [*Goodrich et al.*, 1997].

[1]Centre for Water Systems, College of Engineering, Mathematics and Physical Sciences, University of Exeter, Exeter, UK.
[2]Geography, College of Life and Environmental Sciences, University of Exeter, Exeter, UK.
[3]Southwest Watershed Research Center, United States Department of Agriculture, Tucson, Arizona, USA.

0043-1397/12/2011WR011298

[5] Distributed parameter and initial condition uncertainty is a significant problem in itself [*Yatheendradas et al.*, 2008; *Garcia-Pintado et al.*, 2009], but also confounds the exercise of identifying structural errors within model components that may contribute to overall predictive uncertainty. A renewed focus on reducing model structural uncertainty is evident in the literature [*Refsgaard et al.*, 2006; *Krueger et al.*, 2009], and will be facilitated by the increased availability of high-quality datasets [*Bates et al.*, 2003; *Croft et al.*, 2009]. One uncertain structural component in distributed hydrological models is the channel flow routing component.

[6] In semiarid environments, ephemeral river channels have an increasing effect on catchment hydrological response with an increase in catchment size [*Goodrich et al.*, 1997]. Methods that seek to simulate channel hydrology include: regression relationships between incoming and outgoing discharge [*Walters*, 1990]; and empirically derived routing methods [*Sharma and Murthy*, 1995]. Transmission losses, however, are a nonlinear function of discharge and time [*Mudd*, 2006]. Consequently, explicit routing methods are required to understand how the relationship between inflow discharge and channel characteristics governs infiltration and downstream discharge within ephemeral river reaches [*Goodrich et al.*, 1997].

[7] A number of models have been developed to simulate ephemeral channel rivers explicitly, based on either full [*El-Hames and Richards*, 1998; *Mudd*, 2006] or partial solutions [*Smith et al.*, 1995] of the one-dimensional (1-D) St. Venant equations. Results from numerical and field investigations demonstrate the importance of hydrograph duration [*Parissopoulos and Wheater*, 1991], and channel width [*Goodrich et al.*, 1997; *Mudd*, 2006] in controlling transmission losses in ephemeral channels. The wetted area of the channel bed during flood flows appears to be the primary control on channel transmission losses [*Goodrich et al.*, 1997; *Mudd*, 2006], and therefore the magnitude and duration of the downstream hydrograph. These results demonstrate the importance of accurately parameterizing cross-section shape and the processes governing infiltration in ephemeral channel flow routing models. Existing methods applied to simulate channel flow routing in ephemeral rivers have assumed channel morphology may be approximated by either trapezoidal [*Smith et al.*, 1995] or rectangular (constant width) cross-sections [*El-Hames and Richards*, 1998; *Morin et al.*, 2009]. Trapezoidal and rectangular channels may provide an adequate representation of channel cross-section morphology in single thread reaches. However, ephemeral piedmont rivers of the American Southwest alternate between single thread and braided sections [*Pelettier and DeLong*, 2004]; trapezoidal cross-sections do not adequately represent multiple thread channels. Differences between the simplified cross-section and actual channel morphology will introduce errors into the relationship between stage and wetted perimeter, which will affect flow conveyance and the bed area available for infiltration. In the case of KINEROS [*Smith et al.*, 1995], an empirical correction factor is applied that reduces the effective wetted perimeter of the cross-section that is available for infiltration at low flows. However, there is uncertainty regarding the value that this coefficient should take [*Yatheendradas et al.*, 2008].

[8] A parameter applied to correct for the effect on infiltration of an artificially high wetted perimeter does not account for feedbacks between cross-section shape and flood-wave propagation, a significant factor controlling flood routing [*Hassan*, 1990], even in the absence of transmission losses. In such cases the applied roughness coefficient will need to account for topographic variability not represented by a more explicit definition of cross-section shape, along with other forms of frictional resistance owing to the representation of depth and width using a 1-D approach [*Lane*, 2005]. Assumptions regarding cross-section shape are also likely to have a negative effect on sediment transport estimates derived from such routing models, given that cross-section bed load sediment transport is sensitive to the lateral distribution of flow [*Ferguson*, 2003]

[9] The development and proliferation of topographic datasets derived from light detection and ranging (lidar) technology has facilitated the parameterization of numerical models at a fine spatial resolution (1 m) over increasingly large model domains, for both 1-D models [*Matgen et al.*, 2007; *Aggett and Wilson*, 2009], and also distributed (2-D) flow routing models [*Cobby et al.*, 2001; *Bates et al.*, 2003; *French*, 2003; *Hilldale*, 2007]. A lidar Digital Elevation Model (DEM) offers the potential to constrain cross-section morphology over larger areas than is feasible through ground survey alone, while providing comparable levels of accuracy [*Rayburg et al.*, 2009]. Lidar is particularly useful in ephemeral channels as the channel bed may be surveyed during no-flow conditions, which is not possible in perennial rivers.

[10] High-resolution DEM data available over large areas have the potential to improve the representation of cross-section morphology in 1-D flow routing models applied to ephemeral rivers. However, given other uncertainties surrounding flow routing in these environments, it is unclear whether such data sources can improve the predictive ability of existing 1-D flow routing models. Although manual surveys of similar accuracy have been conducted previously, such information has not often been included in 1-D models. Climatic scenarios point toward a drier climate for the American Southwest, and more frequent, high-intensity rainfall events [*Seager et al.*, 2007]. There is therefore a need to improve the predictive ability of hydrological models applied in such regions, to improve understanding and prediction of flash flood hazard and water resources.

[11] This study will investigate whether incorporating high-resolution (1 m) topography into the structure of a 1-D flow routing model can improve flow routing predictions when applied to an ephemeral river, in comparison to a model using an existing, simplified representation of cross-section morphology. The study has the following research aims: (1) Determine whether the integration of distributed topographic information can improve 1-D flow routing in ephemeral rivers on an event basis (calibration); (2) Identify how improved topographic representation modifies model structure and affects model parameter uncertainty; (3) Evaluate whether modifications to 1-D model structure, and the increase in topographic information contained within the model can improve model predictive ability (evaluation).

2. Modeling Strategy: Kinematic Wave Model

[12] To address the research aims a 1-D kinematic flow routing model was applied to simulate runoff events along

the main channel of the Walnut Gulch Experimental Watershed (WGEW) [*Renard et al.*, 2008]. The flow routing model was applied using two alternative model structures: First, using a trapezoidal representation of cross-section morphology (K-Tr); Second, using laterally distributed cross-section morphology derived from a 1 m lidar derived DEM (K-Li).

[13] The l-D kinematic wave equation, which has been widely applied to simulate flow in ephemeral channels [*Garcia-Pintado et al.*, 2009; *Morin et al.*, 2009; *Smith et al.*, 1995; *Yatheendradas et al.*, 2008], is applied here and solved at each cross-section in the model domain using an explicit scheme:

$$A_i^{t+1} = A_i^t - \frac{\Delta t}{\Delta x}(Q_i^t - Q_{i-1}^t) - q_i \Delta t, \tag{1}$$

where A is the flow cross-section area (m^2); t is time (s), and subscript i is cross-section; Q is discharge ($m^3\ s^{-1}$) calculated from A using the Manning equation with Manning's coefficient, n; x is distance in the stream-wise direction (m); and q represents transmission losses ($m^2\ s^{-1}$), which are determined at each cross-section by calculating the sum of infiltration across all wet cross-section cells. Infiltration rate (I) in each cell is calculated using the Green-Ampt equation [*Green and Ampt*, 1911], capable of simulating run on infiltration:

$$I = K_s \frac{w + z + h}{z}, \tag{2}$$

where I is infiltration rate ($m\ s^{-1}$), K_s is saturated hydraulic conductivity ($m\ s^{-1}$), w is the wetting front suction (m), z is accumulated depth of infiltration (m) in the cell, and h is the depth of water at the bed surface (m). Infiltration in K-Tr is calculated using the empirical correction factor applied in KINEROS(2), which uses an effective wetted perimeter (p_e) to correct for the error introduced in the actual wetted perimeter (a) when calculating infiltration in trapezoidal cross-sections [*Smith et al.*, 1995]:

$$p_e = \min\left[\frac{h}{Wc\sqrt{BW}}, 1\right] a, \tag{3}$$

where BW is the channel bottom width (m), and Wc is the empirical Woolhiser coefficient. In K-Tr simulations, cross-section cells are ordered from minimum elevation to the maximum elevation, and p_e is used to determine the fraction of wet cells to calculate infiltration, which are then summed to determine q.

3. Study Area and Data

[14] The research aims were addressed using data derived from The WGEW, southeast Arizona, USA (31.45°N, 110.0°W; Figure 1; see WRR special issue) [*Moran et al.*, 2008]. The watershed, with an area of 150 km^2, drains west from headwaters in the Dragoon Mountains in the east (1900 m amsl) into the San Pedro River (1250 m amsl). The main channel of The WGEW is a 6.5 km continuous sand bed river, which alternates between single thread reaches and braided sections with a wavelength >200 m (Figure 2). The reach may be considered typical of river morphologies present on Piedmont slopes of the basin and range province of the semiarid American Southwest [*Pelettier and DeLong*, 2004].

[15] Lidar data used to determine channel cross sections for the l-D model were acquired from an OPTECH ALTM 1233 (Optech Incorporated, Toronto, Canada) laser scanner flown over The WGEW in the summers of 2003 and 2004. The Optech ALTM 1233, which has a 1064 nm laser, a pulse rate of 33 kHz, a scanning frequency of 28 Hz, and a scanning angle of ±20°, was flown to obtain a spot size of approximately 15 cm, and the data processed using Optech REALM proprietary software, alongside a vegetation filtering algorithm [*Hutton*, 2010], to derive a 1 m resolution DEM of the watershed. The DEM had a vertical accuracy of ±0.15 m derived in comparison to ground based differential GPS survey points measured in 2003 at Flumes 1 and 2, and also using stable locations at surveyed cross-sections in the reach.

[16] Analysis of the 1 m channel DEM was used to determine where to extract representative cross-sections of the channel morphology. The 101 cross-sections were extracted manually from the DEM at a spacing of ~65 m, a spacing sufficient to represent changes between braided and single

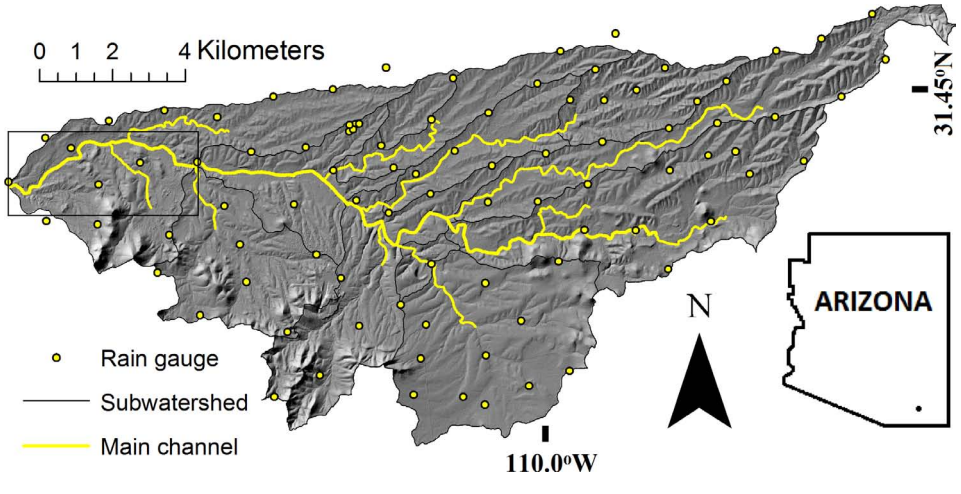

Figure 1. Hillshade map of the Walnut Gulch Experimental Watershed, SE Arizona. The main channel reach under study is enclosed in the black rectangle, as shown in Figure 2.

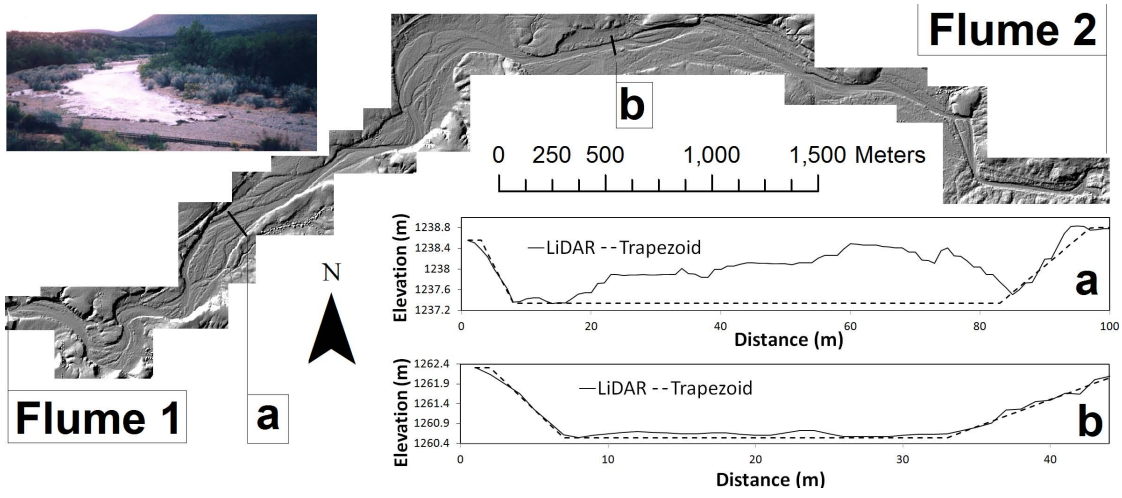

Figure 2. Lidar derived DEM hillshade showing downstream changes between braided and single thread morphology, and two representative cross-sections. Note exaggerated Y-Axis. The upper-left photograph shows a flash flood event looking upstream from Flume 1.

thread sections in the reach, which alternate downstream with an approximate wavelength of >200 m (Figure 2). Trapezoid cross-sections were constructed directly from the lidar data: the channel bottom elevation in each cross section was set to the elevation of the thalweg identified from the lidar data; trapezoidal cross sections were fitted by varying the channel bottom width to reduce the mean-square-error between the original cross section data and the trapezoidal cross section (Figure 2).

[17] Five discrete flow events recorded at Flume 2 and Flume 1 upstream and downstream of the study reach, respectively, were used to address the research aims (Table 1). The selected events first activated Flume 2 and then Flume 1 with little or no rainfall recorded in the tributary catchments that join the main reach between the flumes (Figure 1). These events were therefore chosen to ensure mass conservation when calculating both infiltration in the reach, and the downstream hydrograph at Flume 1.

4. Model Evaluation

[18] The model evaluation procedure employed to address the research aims follows the concepts outlined within the Generalized Likelihood Uncertainty Estimation (GLUE) methodology [*Beven and Binley*, 1992; *Brazier et al.*, 2000], which is applied to understand how different parameter sets (and interactions) within competing models structures affect model performance [e.g., *Beven and Freer*, 2001].

[19] Each model structure (K-Tr and K-Li) was applied to simulate the events listed in Table 1. For each model application to an event, 40,000 Monte Carlo simulations were conducted sampling randomly from uniform prior distributions for each parameter (Table 2). Prior ranges were determined with recourse to studies within similar sand-gravel ephemeral channels [*Al-Qurashi et al.*, 2008; *Blasch et al.*, 2006; *Dahan et al.*, 2007; *El-Hames and Richards*, 1998; *Michaud and Sorooshian*, 1994; *Morin et al.*, 2009; *Yatheendradas et al.*, 2008], and hydrological properties for the bed sediment texture [*Rawls et al.*, 1993]. After 20,000 simulations the initial parameter ranges were narrowed where no well performing parameter sets were found across all events (Table 2). For each event an evaluation of the convergence of the Cumulative Distribution Functions (CDF) across each parameter range for each measure of model performance demonstrated 40,000 simulations were sufficient for convergence of the posterior distribution.

[20] In order to identify model structures and parameter combinations that perform well for the right hydrological reasons [*Brazier et al.*, 2000], four performance measures (PM) have been chosen to evaluate model performance, calculated for each event simulation (Table 3). The fourth PM (NT) is derived by multiplying the values of all other performance measures to define a good model prediction as one which replicates the magnitude and timing of discharge (NP), and the shape of the hydrograph (NSE), while also maintaining the correct mass balance (e.g., predict transmission losses

Table 1. Summary Discharge Statistics of Runoff Events Used in Model Evaluation[a]

	Flume 2		Flume 1		
Event Number and Date	Q Total (m^3)	Q Peak ($m^3\ s^{-1}$)	Q Total (m^3)	Q Peak ($m^3\ s^{-1}$)	Q Loss (m^3(%))
1. 17 Jul 1999	71,191	12.6	42,572	12.6	28,619 (40)
2. 23 Jul 1999	261,147	61.2	238,838	61.1	22,309 (9)
3. 22 Aug 2005	54,498	12.7	46,587	6.3	7911 (15)
4. 10 Sep 2006	36,202	9	16,227	4.2	19,975 (55)
5. 25 Jul 2007	28,604	7.7	11,169	3.6	17,435 (60)

[a]Summary Discharge is Q.

Table 2. Parameter Ranges Used in Monte Carlo Simulation for Each Model Structure[a]

Parameter	K-Li	K-Tr
Manning (n;)	0.015–0.1 (0.015–0.05)	0.015–0.1 (0.015–0.05)
Initial moisture (M;%)	0–1	0–1
Saturated Conductivity (K_s; mm h^{-1})	1.8–432 (1.8–144)	1.8–432
Wetting Front Suction (W_{fs}; m)	0.0009–0.1	0.0009–0.1
Woolhiser Coefficient (W_c)	–	0–0.45

[a]Ranges in brackets show narrowed ranges sampled during the final 20,000 simulations based on behavioral simulations found in the first 20,000 simulations.

correctly) at Flume 1 (NV). A value of 1 for all of the measures considered above indicates a perfect fit. All simulations that produce a value less than zero are considered nonbehavioral for that performance measure, and are given a value of zero.

[21] In order to provide reach specific context to evaluate the quality of model performance, and determine how well each model can simulate the reach transfer function between the upstream and downstream hydrograph, benchmark values for NSE and NP are derived following *Shaefli and Gupta* [2007]. However, instead of adjusting input rainfall, the input hydrographs for each event are multiplied by the runoff ratio (Flume 1 volume divided by Flume 2 volume) and adjusting by an optimum lag which minimizes the value of NSE and NP separately for each event compared to the respective hydrograph at Flume 1.

[22] A global method, Regional Sensitivity Analysis (RSA) [*Brazier et al.*, 2007; *Freer et al.*, 1996; *Hornberger and Spear*, 1981], is applied to evaluate model sensitivity. To overcome the problems of specifying a single restrictive behavioral threshold, and to address the second research aim, model sensitivity is evaluated by calculating the CDF for each performance measure as a function of each model parameter for the top 10% and also top 50% of model simulations when applied to each event. RSA sensitivity scores are derived by calculating the difference in area between the uniform prior CDF and that of the posterior CDF for each parameter. The range of each parameter is normalized when calculating the aerial difference to compare sensitivity across parameters, which therefore has a maximum value of 0.5. To supplement the RSA sensitivity analysis, which only considers first-order sensitivity, the strength of linear relationships between parameters for the top performing 500 parameter sets, based on NT, were also evaluated.

Table 3. Performance Measures Used in Model Evaluation

Name	Equation[a]
Nash-Sutcliffe (NSE)	$\max\left(1-\frac{\sum_{i=1}^{T}(Q_o^t-Q_s^t)^2}{\sum_{i=1}^{T}(Q_o^t-\overline{Q}_o)^2},0\right)$
Normalized Peak (NP)	$\max\left(\left(1-\frac{\lvert Q_{ps}-Q_{po}\rvert}{Q_{po}}\right)*\left(1-\frac{\lvert T_{ps}-T_{po}\rvert}{T_{po}}\right),0\right)$.
Normalized Volume (NV)	$\max\left(1-\frac{\lvert V_s-V_o\rvert}{V_o},0\right)$
Normalized Total (NT)	NSE + NP + NV

[a]Q^t = discharge at time t; $\overline{Q}$ = mean event discharge; Q_p = peak discharge; V = total event volume; T_p = time of peak discharge; subscripts o and s refer to observed and simulated, respectively.

[23] To address the third research objective and identify whether K-Li can outperform K-Tr when a single parameter set is applied across runoff events, the PM scores for each parameter set are summed across events and renormalized to 1, allowing a parameter set to perform poorly for an event, yet still score well overall for good performance across all other events [*Yatheendradas et al.*, 2008].

5. Results

5.1. Event Based Model Performance

[24] A comparison of the optimal PM scores derived when applying each model structure to each runoff event (Table 4), show that for four events K-Li outperforms K-Tr in terms of total performance (NT). K-Tr produces a better overall performance for Event 3, however both models outperform the benchmark models (BM) for this event, therefore both capture aspects of the reach transfer function that is not present in the input hydrograph. For all events both models outperform the NP BM, and can produce near optimal peak discharge predictions (NP $>$ 0.96). Neither model can outperform the NSE score for Event 2, and K-Tr is also worse than NSE BM for Events 4 and 5. Both models are capable of producing near perfect mass balance for each event when considered only in terms of the NV performance measure. The NT scores for each event are less than the product of the optimal scores for NSE, NP and NV; therefore the optimal NT score is not produced from a single parameter set that produces optimal scores for all other performance measures.

5.2. Sensitivity Analysis

[25] Based on the RSA sensitivity scores for all events and performance measures calculated for the top 10% of parameter sets (Table 5), K-Li is most sensitive to K_s followed by n (except NSE for Event 1), and like the K-Tr model, insensitive to the initial moisture (M) and wetting front suction (w_{fs}). The lowest n sensitivity scores in both models for NV show the correct runoff volume may be predicted without necessarily producing the hydrograph shape, as measured by NSE. In K-Tr the single dominant parameter is n, with the exception of NV for Event 5. The next most sensitive parameters were K_s and W_c. Some of the largest K_s sensitivity scores for the T model occurred in Event 2, the largest runoff event. The results obtained using the top 50% of behavioral parameter sets (not shown) identified the same ordering of the most sensitive parameters.

[26] For K-Li, significant positive linear interactions were identified between M and K_s, except for Event 3 (Table 6), and between n and M, except for Events 2 and 3. Given RSA identifies optimal K_s and n in a narrow area in parameter space, such interactions are of secondary importance. In K-Tr for all events except Event 2, a significant positive interaction was identified between K_s and W_c, which coupled with low RSA scores shows this interaction for the optimal performing parameter sets occurs across the whole range sampled for each parameter. Significant positive interactions between n and both K_s and W_c were identified when K-Tr was applied to Event 3.

Table 4. Performance Measures for the Optimal Performing Parameter Sets for Each Runoff Event and Model Structure[a]

	NSE			NP			NV		NT	
Event Number and Date	K-Li	K-Tr	BM	K-Li	K-Tr	BM	K-Li	K-Tr	K-Li	K-Tr
Event 1: 17 Jul 1999	**0.965**	0.964	0.857	0.984	**0.998**	0.613	0.999	0.999	**0.744**	0.651
Event 2: 23 Jul 1999	0.978	0.969	**0.983**	**0.963**	0.960	0.913	0.999	0.999	**0.911**	0.882
Event 3: 22 Aug 2005	0.943	**0.962**	0.684	**0.997**	0.994	0.274	0.999	0.999	0.634	**0.763**
Event 4: 10 Sep 2006	**0.986**	0.978	0.985	0.991	**0.998**	0.953	0.999	0.999	**0.900**	0.811
Event 5: 25 Jul 2007	**0.991**	0.943	0.964	0.990	**0.995**	0.845	0.999	0.999	**0.955**	0.769
Total	**0.862**	0.845	–	**0.868**	0.863	–	0.884	**0.885**	**0.662**	0.598

[a]BM refers to predictions derived from the benchmark model. The bolded scores show the best performing model for each measure of model performance.

5.3. Predictive Performance

[27] K-Li outperformed K-Tr when measured by NSE, NP and NT (Table 4) when parameter sets were evaluated across events, and produced a number of better performing parameter sets (Figure 3). Sensitivity across all events confirms the sensitivity results identified for each individual event (Table 4; Figure 3): K-Li performance across all events is most sensitive to K_s and Manning's n, with optimal parameter sets in the range 7–46 mm h^{-1}, and 0.02–0.03, respectively. All event optimal values of K_s and n lie in these ranges, except Event 2, which had a higher roughness coefficient (0.035). The lack of significant relationships in K-Li across all events for M, alongside the spread in the optimal initial moisture for each event (Figure 3), suggests M is specific to each event. The sensitivity to n across events for K-Tr is also shown in Figure 3; the optimal value is smaller than in K-Li (0.015–0.023), and like K-Li all event optimal values of n lie in this range, except for Event 2. The strong linear relation between W_c and K_s in K-Tr predictions was also identified for total model performance across all events. In contrast to K-Li predictions, optimal performing parameter sets can be found across the whole range of K_s, which is also the case for M and W_c. Although, the best performing parameter sets are toward the lower range of W_c.

[28] Narrower clustering of the top 500 parameter sets in K-Li model (Figure 4) shows the larger number of optimal performing parameter sets, compared to K-Tr, particularly for Event 1 and 2. However this is not the same for Event 3, where K-Tr outperforms K-Li, most notably around the second hydrograph peak. For Event 1 and Event 2 both models struggle to predict peak discharge in evaluation. When both models were calibrated to NP, peak discharge can be predicted well, which in the case of Event 1 results in an over prediction of the receding hydrograph limb. The time to the rising limb is well predicted for all other events, and is marginally better in K-Li predictions for Event 4 and Event 5. For these events K-Li also performs better during the receding hydrograph limbs, notably in Event 5.

Table 5. RSA Sensitivity Scores Derived From the Top 10% of Parameter Sets When Each Model Was Applied to Each Event for Each Measure of Model Performance[a]

	K-Li				K-Tr				
PM	n	W_{fs}	M	K_s	n	W_{fs}	M	K_s	W_c
				Event 1					
NSE	**0.436**	0.003	0.049	*0.405*	**0.469**	0.003	0.023	0.046	*0.134*
NP	*0.391*	0.006	0.095	**0.452**	**0.425**	0.006	0.039	*0.254*	0.186
NV	*0.268*	0.004	0.047	**0.444**	**0.180**	0.010	0.014	0.024	*0.120*
NT	*0.426*	0.003	0.058	**0.427**	**0.465**	0.004	0.013	0.012	*0.107*
				Event 1					
NSE	*0.309*	0.005	0.057	**0.415**	**0.371**	0.011	0.051	*0.203*	0.120
NP	*0.302*	0.006	0.129	**0.450**	**0.327**	0.008	0.081	*0.360*	0.117
NV	*0.283*	0.005	0.069	**0.474**	**0.278**	0.007	0.132	*0.390*	0.117
NT	*0.296*	0.005	0.087	**0.455**	**0.344**	0.011	0.083	*0.330*	0.129
				Event 3					
NSE	*0.358*	0.005	0.023	**0.458**	**0.451**	0.004	*0.014*	0.069	*0.165*
NP	*0.402*	0.004	0.074	**0.407**	**0.443**	0.005	0.007	0.022	*0.144*
NV	*0.273*	0.006	0.059	**0.476**	**0.312**	0.006	0.040	*0.305*	0.214
NT	*0.357*	0.006	0.025	**0.463**	**0.447**	0.003	0.006	0.062	*0.176*
				Event 4					
NSE	*0.373*	0.004	0.023	**0.413**	**0.449**	0.005	0.006	*0.054*	0.053
NP	*0.379*	0.004	0.056	**0.408**	**0.421**	0.004	0.003	*0.099*	0.073
NV	*0.275*	0.005	0.055	**0.444**	**0.091**	0.004	0.028	0.043	*0.069*
NT	*0.369*	0.004	0.024	**0.425**	**0.448**	0.003	0.006	*0.104*	0.099
				Event 5					
NSE	*0.379*	0.004	0.026	**0.415**	**0.453**	0.005	0.008	*0.065*	0.056
NP	*0.381*	0.007	0.061	**0.419**	**0.424**	0.007	0.005	0.069	*0.088*
NV	*0.273*	0.005	0.050	**0.438**	0.043	0.006	0.028	0.083	*0.071*
NT	*0.379*	0.004	0.028	**0.425**	**0.460**	0.005	0.012	0.105	*0.135*
				Total					
NSE	*0.381*	0.003	0.023	**0.425**	**0.452**	0.006	0.007	0.020	*0.086*
NP	*0.379*	0.005	0.069	**0.424**	**0.428**	0.008	0.007	0.017	*0.110*
NV	*0.274*	0.004	0.047	**0.448**	**0.206**	0.003	0.009	0.131	*0.158*
NT	*0.373*	0.005	0.039	**0.441**	**0.452**	0.005	0.007	0.015	*0.083*

[a]Total shows values across events. PM is model performance. Bold and italic indicates, respectively, the most sensitive parameter (bold), and second most sensitive parameter (italic), for each model and performance measure.

Table 6. Significant Linear Relationships Between Parameters Determined From the Top 500 Parameter Sets for Each Event and Model as Measured With NT[a]

	K-Li		K-Tr	
Event Number and Date	Parameters	R^2	Parameters	R^2
Event 1: 17 Jul 1999	n-M	+0.17	W_c-K_s	+0.72
Event 1: 17 Jul 1999	M-K_s	+0.41	–	–
Event 2: 23 Jul 1999	M-K_s	+0.16	–	–
Event 3: 22 Aug 2005	n-K_s	−0.17	W_c-K_s	+0.47
Event 3: 22 Aug 2005	–	–	n-K_s	+0.14
Event 3: 22 Aug 2005	–	–	W_c-n	+0.63
Event 4: 10 Sep 2006	M-K_s	+0.52	W_c-K_s	+0.75
Event 4: 10 Sep 2006	n-M	+0.15	–	–
Event 5: 25 Jul 2007	n-M	+0.21	W_c-K_s	+0.7
Event 5: 25 Jul 2007	M-K_s	+0.55	–	–
Total	–	–	W_c-K_s	+0.77

[a]For the values, $p < 0.01$.

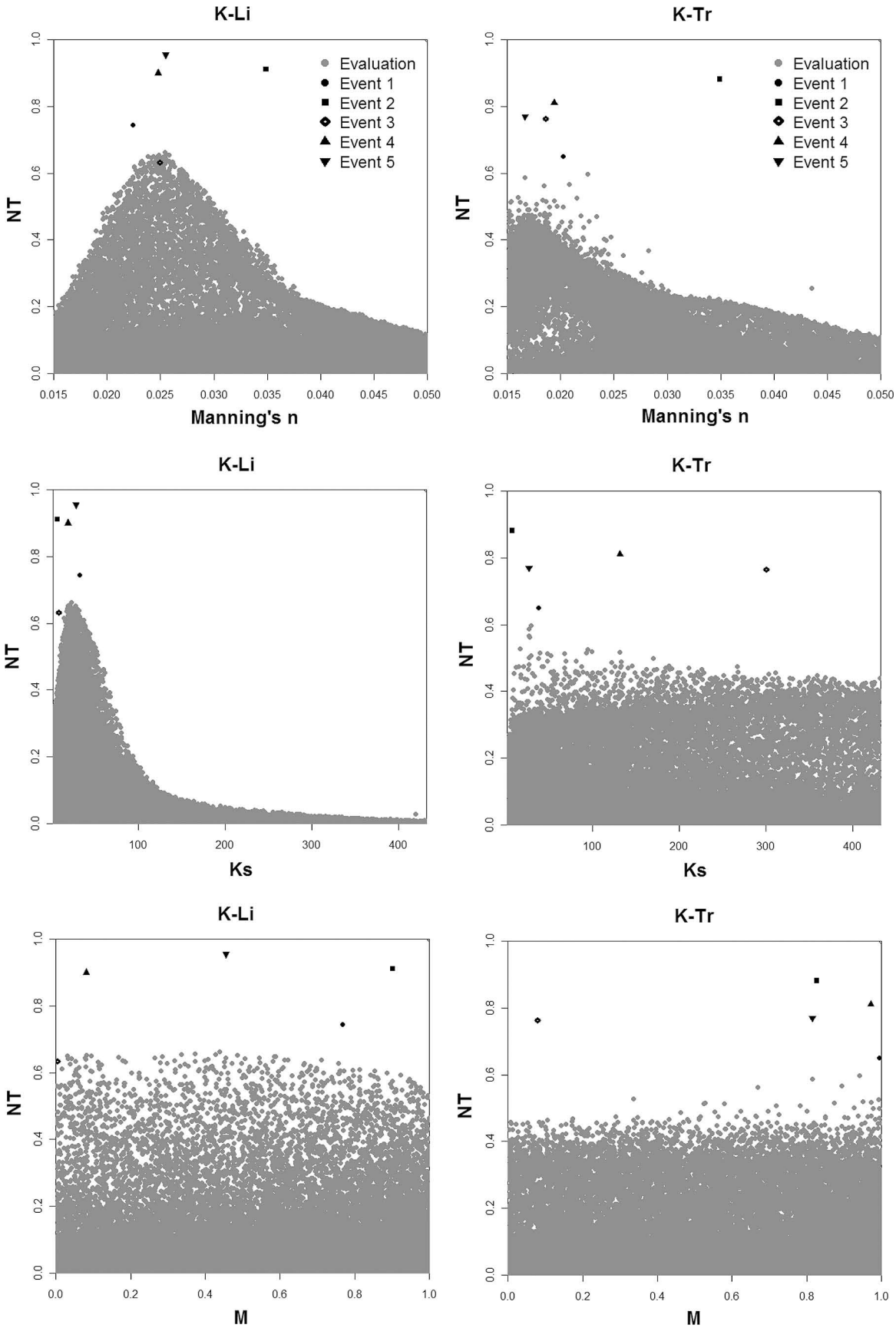

Figure 3. Dotty plots showing total model performance (NT) as a function of the most sensitive parameters when each parameter set was applied to all runoff events (evaluation), and the optimal performing parameter when each model was calibrated to each calibrated to each individual event.

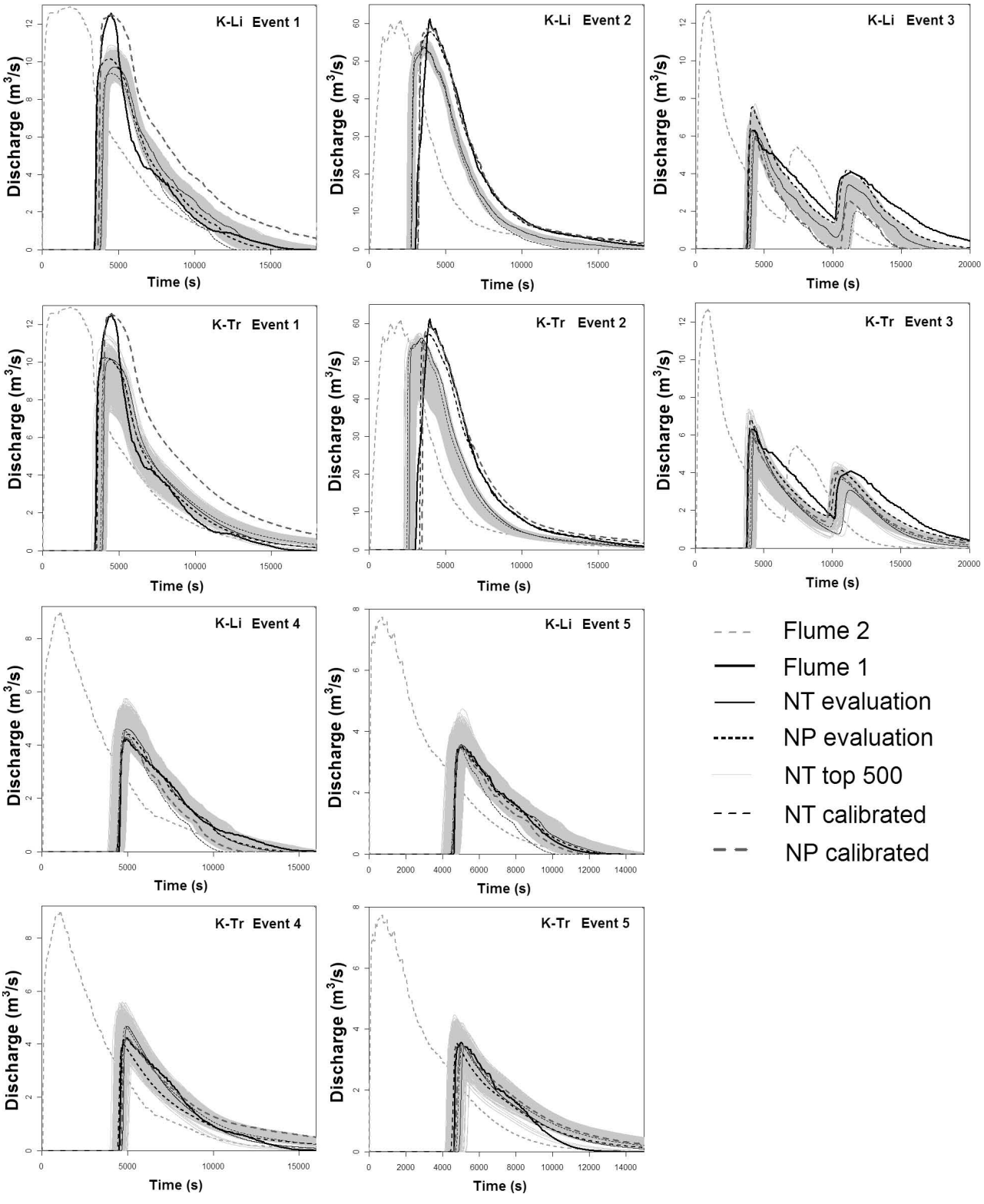

Figure 4. Hydrograph plots showing the optimal performing model predictions of both models (K-Li and K-Tr) in comparison to 5 runoff events at Flume 1 in both calibration and evaluation, as measured by NT and NP. The figures also show the top 500 performing parameter sets in evaluation, as measured by NT when performance was evaluated across events.

6. Discussion

[29] The integration of distributed topographic information into the K-Li model, in the form of lidar derived elevations, generally improves model performance compared to K-Tr when the models are calibrated to individual events, and also when applied across events, producing more behavioral simulations. The exception to this is for Event 3, where K-Tr performs better in predicting both hydrograph peaks. However, both models significantly outperform the benchmark model for this event.

[30] The sensitivity analysis conducted to address the second research aim supports the conclusion that K-Li is a better model for future event prediction in comparison to K-Tr. In the former model, the two most sensitive parameters K_s and n are similar when calibrated to each event, and in evaluation when applied across events. The exception to this is the calibrated n for Event 2, which was the largest event considered, and had a peak discharge approximately five times the size of the next largest event. Event 2 would have inundated a much larger area of the channel and floodplains, and also inundated more of the vegetation that has developed within and alongside the channel over the last 40 years [*Nichols and Shipek*, 2006]. The event, therefore, required a higher roughness coefficient to reflect these conditions. In the other events the optimal range for n was 0.020–0.030, which is consistent with literature values for clean, straight channels [*Chow*, 1959]; i.e., the main inset channel in Walnut Gulch. In future application aerial imagery of the channel, alongside the unfiltered lidar DEM, may be used to distinguish vegetated from bare channel areas, and allow calibration of roughness coefficients both for the channel and vegetated floodplain.

[31] In K-Li the optimal infiltration values in both calibration and evaluation are between 7 and 46 mm h^{-1}. Although these infiltration rates are within the wide range of saturated infiltration rates (1.2–254 mm h^{-1}) recorded for comparable rivers of the American Southwest [*Hoffman et al.*, 2002; *Constantz et al.*, 2003; *Blasch et al.*, 2006], they are lower than that recorded for this channel in previous experiments [*Coes and Pool*, 2005]. *Dahan et al.* [2007] found infiltration rates recorded during a natural flow event were typically lower than those recorded by ring infiltrometers and ponding experiments. Lower infiltration rates during natural flow events may result from air escaping at the flood bore wave [*Hassan*, 1990], and the presence of abundant fine sediment near to the channel bed that may impede infiltration [*Lange*, 2005]. Such processes are not currently represented in existing infiltration models, and might be accounted for indirectly by changes in other parameter values (e.g., K_s). Further work is required to understand the effect of these factors on infiltration.

[32] The initial moisture content (M) had a secondary influence on model performance on an event basis through interactions with other model parameters in K-Li. Events 1 and 2, which both maintained their peak discharges, occurred in a period of frequent channel activity. In contrast, Event 4 and Event 5 were preceded by little channel activity. These data suggest that the initial moisture content may be important in reducing infiltration rates near the peak, and that model results may be improved by incorporation of a moisture model dependent on recent channel activity. However, as the first two events had the largest transmission losses, a greater understanding is required of how reduced peak infiltration leads to greater cross-section inundation downstream and therefore increasing infiltration. Infiltration is calculated separately in each cell that constitutes the channel cross-section in K-Li, which in contrast to a laterally lumped approach means that each newly inundated cross-section cell simulates higher transient infiltration rates associated with an initially dry bed [*Blasch et al.*, 2006]. The model is therefore more representative of the physical conditions and complex dynamics governing transmission losses.

[33] The optimal performing parameter sets across events in K-Tr were toward the lower range for n. In the braided sections of the main channel a trapezoidal cross-section provides a poor approximation of the true morphology (Figure 2). The higher wetted perimeter therefore requires a lower and less physically realistic roughness coefficient to convey the flood discharge. Strong parameter interactions within K-Tr were identified between K_s, and W_c. The compensatory effect of these parameters on the rate of infiltration resulted in optimal parameter sets in different areas of parameter space for all events considered. The result is that it is difficult to infer the physical meaning of the W_c, and for predictive purposes, optimize or "fix" K-Tr parameters for future application. It is possible to fix W_c at the default value (0.15) applied in a number of KINEROS(2) applications [*Smith et al.*, 1995], which gives slightly worse optimal predictions than those found in this study (Table 4), and results in optimal infiltration rates in the range 5–223 mm h^{-1}. While the upper end of this range might seem physically more realistic than the optimal values found in K-Li (7–46 mm h^{-1}), they are obtained by applying an empirical derived, and poorly justified parameter value. Whereas in K-Li the optimal range of K_s values are found with a physically more plausible, and distributed representation of the effects of cross-section morphology on flow routing.

[34] A number of studies have identified the lack of transferability of parameter values between event predictions when used in semiarid hydrological models [*Al-Qurashi et al.*, 2008; *Yatheendradas et al.*, 2008], and the need to take an event based approach to understand/predict semiarid hydrological response [*Knighton and Nanson*, 2001; *Wainwright et al.*, 2008; *Garcia-Pintado et al.*, 2009]. The consistency of parameters in K-Li suggests, alongside recourse to aerial imagery and consideration of previous events, predictions from this model are more robust for further application than identified in previous studies.

[35] Data available for this study allowed focus on a particular structural element of distributed catchment models, which led to development of a better understanding of parameter interactions, detection of model structural deficiencies, and identification of where advances in data collection may improve model application. Such model limitations are difficult to infer from whole-of-catchment model applications due to the compensatory effects of errors in hillslope model structure, input data and parameters, which may lead to the identification of erroneous parameter values [*Yatheendradas et al.*, 2008; *Bahat et al.*, 2009]. The issue is analogous to the problems of the sediment delivery

concept [*Parsons et al.*, 2006] as it highlights the limitations of inferring catchment understanding from a single integrated measure of catchment response. Improved data availability to constrain individual catchment components, both qualitative [e.g., *McMillan and Clark*, 2009] and quantitative (as implemented here), can improve the parameter inference procedure, leading to more robust models and more robust model predictions.

7. Conclusion

[36] The objective of this paper was to investigate whether lidar-derived data could lead to improved prediction of flow events in ephemeral channels. In general, K-Li showed improved performance in comparison to K-Tr, both when each model was calibrated to individual events and during an evaluation phase when the models (and parameter sets) were applied across events. Sensitivity analysis identified that the K-Li model also had greater consistency in behavioral parameter sets across runoff events, with optimal parameter values for the most sensitive parameters (saturated infiltration and the roughness coefficient) occurring for all events in a narrower region of parameter space. In contrast, parameter interaction within K-Tr resulted in poorly constrained behavioral parameter sets across parameter space. Interaction between Saturated Infiltration (K_s) and the Woolhiser Coefficient (W_c), which has little physical meaning, had a compensatory effect on model performance. Data used in this study allowed focus on a particular structural element common in distributed catchment models. An understanding of the channel model component, as developed here, has previously been dominated by uncertainty in input conditions and other catchment components. These results suggest that lidar derived cross-section morphology can lead to improved, and more robust flash flood prediction, particularly in distributed catchment models where the channel component can dominate runoff response.

[37] **Acknowledgments.** The research was primarily funded by a University of Exeter Graduate Fellowship, awarded to the first author. Significant support was also provided by The USDA-ARS Southwest Watershed Research Center.

References

Aggett, G. R., and J. P. Wilson (2009), Creating and coupling a high-resolution DTM with a 1-D hydraulic model in a GIS for scenario-based assessment of avulsion hazard in a gravel-bed river, *Geomorphology*, *113*(1–2), 21–34.

Al-Qurashi, A., N. McIntyre, H. Wheater, and C. Unkrich (2008), Application of the Kineros2 rainfall-runoff model to an arid catchment in Oman, *J. Hydrol.*, *355*, 91–105.

Ashley, S. T., and W. S. Ashley (2008), Flood fatalities in the United States, *J. Appl. Meteorol. Climatol.*, *47*, 805–818.

Bahat, Y., T. Grodek, J. Lekach, and E. Morin (2009), Rainfall-runoff modeling in a small hyper-arid catchment, *J. Hydrol.*, *373*(1–2), 204–217.

Bates, P. D., K. J. Marks, and M. S. Horritt (2003), Optimal use of high-resolution topographic data in flood inundation models, *Hydrol. Processes*, *17*, 537–557.

Beven, K., and A. M. Binley (1992), The future of distributed models: Model calibration and uncertainty estimation, *Hydrol. Processes*, *6*, 279–298.

Beven, K., and J. Freer (2001), A dynamic TOPMODEL, *Hydrol. Processes*, *15*, 1993–2011.

Blasch, K. W., T. P. A. Ferre, J. P. Hoffmann, and J. B. Fleming (2006), Relative contributions of transient and steady state infiltration during ephemeral streamflow, *Water Resour. Res.*, *42*, W08405, doi:10.1029/2005WR004049.

Brazier, R. E., K. J. Beven, J. Freer, and J. S. Rowan (2000), Equifinality and uncertainty in physically based soil erosion models: Application of the glue methodology to WEPP-the water erosion prediction project-for sites in the UK and USA, *Earth Surf. Processes Landforms*, *25*(8), 825–845.

Brazier, R. E., A. J. Parsons, J. Wainwright, D. M. Powell, and W. H. Schlesinger (2007), Upscaling understanding of nitrogen dynamics associated with overland flow in a semi-arid environment, *Biogeochemistry*, *82*(3), 265–278.

Burnash, R. J. C. (1995), The NWS River Forecast System, in *Computer Models of Watershed Hydrology*, edited by V. P. Singh, pp. 311–366, Water Resour. Publ., Highlands Ranch, Colo.

Chow, V. T. (1959), *Open-Channel Hydraulics*, McGraw-Hill, London.

Cobby, D. M., D. C. Mason, and I. J. Davenport (2001), Image processing of airborne scanning laser altimetry data for improved river flood modelling, *ISPRS J. Photogramm. Remote Sensing*, *56*(2), 121–138.

Coes, A. L., and D. R. Pool (2005), Ephemeral-stream channel and basin-floor infiltration and recharge in the Sierra Vista subwatershed of the upper San Pedro Basin, Southeastern Arizona, *USGS Prof. Pap. 1703*, 67 pp., U.S. Geological Survey, NW Washington, DC.

Constantz, J., S. W. Tyler, and E. Kwicklis (2003), Temperature-profile methods for estimating percolation rates in arid environments, *Vadose Zone J.*, *2*, 12–24.

Croft, H., K. Anderson, and N. Kuhn (2009), Characterizing soil surface roughness using a combined structural and spectral approach, *J. Soil Sci.*, *60*, 431–442.

Dahan, O., Y. Shani, Y. Enzel, Y. Yechieli, and A. Yakirevich (2007), Direct measurements of floodwater infiltration into shallow alluvial aquifers, *J. Hydrol.*, *344*, 157–170.

El-Hames, A. S., and K. S. Richards (1998), An integrated, physically based model for arid region flash flood prediction capable of simulating dynamic transmission loss, *Hydrol. Processes*, *12*(8), 1219–1232.

Ferguson, R. I. (2003), The missing dimension: Effects of lateral variation on 1-D calculations of fluvial bedload transport, *Geomorphology*, *56*, 1–14.

Foody, G. M., E. M. Ghoneim, and N. W. Arnell (2004), Predicting locations sensitive to flash flooding in an and environment, *J. Hydrol.*, *292*(1–4), 48–58.

Freer, J., K. Beven, and B. Ambroise (1996), Bayesian estimation of uncertainty in runoff production and the value of data: An application of the GLUE approach, *Water Resour. Res.*, *32*, 2161–2173.

French, J. R. (2003), Airbourne Lidar in support of geomorphological and hydraulic modelling, *Earth Surf. Processes Landforms*, *28*, 321–335.

Garcia-Pintado, J., G. G. Barbera, M. Erena, and V. M. Castillo (2009), Calibration of structure in a distributed forecasting model for semiarid flash flood: Surface storage and channel roughness, *J. Hydrol.*, *377*, 165–184.

Goodrich, D. C., L. J. Lane, R. M. Shillito, S. N. Miller, K. H. Syed, and D. A. Woolhiser (1997), Linearity of basin response as a function of scale in a semiarid watershed, *Water Resour. Res.*, *33*(12), 2951–2965.

Green, A., and G. A. Ampt (1911), Studies on soil physics: 1. Flow of air and water through soils, *J. Agic. Sci.*, *4*, 1–24.

Hassan, M. A. (1990), Observations of desert flood bores, *Earth Surf. Processes Landforms*, *15*(5), 481–485.

Hilldale, R. C. (2007), Using bathymetric LiDAR and a 2-D hydraulic model to quantify aquatic habitat, paper presented at Proceeding if the ASCE World Environmental and Water Resources Congress, Tampa, Fla., 15–17 May.

Hoffman, J. P., M. A. Ripich, and K. M. Ellett (2002), Characteristics of shallow deposits beneath Rillito Creek, Pima County, Arizona, *U.S. Geol. Surv. Water Resour. Invest. Rep., 01-4257*, 51 pp., U.S. Geological Survey, NW Washington, DC.

Hooke, J. M., and J. M. Mant (2000), Geomorphological impacts of a flood event on ephemeral channels in SE Spain, *Geomorphology*, *34*(3–4), 163–180.

Hornberger, G. M., and R. Spear (1981), An approach to the preliminary analysis of environmental systems, *J. Environ. Manage.*, *12*, 7–18.

Hutton, C. J. (2010), Modelling watershed processes in semi-arid environments, PhD dissertation, Coll. of Life and Environ. Sci., Univ. of Exeter, U. K.

Knighton, A. D., and G. C. Nanson (2001), An event based approach to the hydrology of arid zone rivers in the Channel Country of Australia, *J. Hydrol.*, *254*(1–4), 102–123.

Krueger, T., J. N. Quinton, J. M. Freer, J. A. Macleod, G. S. Bilotta, R. E. Brazier, P. Butler, and P. M. Haygarth (2009), Uncertainties in data and models to describe dynamics of agricultural sediment and phosphorus transfer, *J. Environ. Qual.*, *38*, 1137–1148.

Lane, S. N. (2005), Roughness—Time for re-evaluation?, *Earth Surf. Processes Landforms*, *30*, 251–253.

Lange, J. (2005), Dynamics of transmission losses in a large arid stream channel, *J. Hydrol.*, *306*, 112–126.

Matgen, P., G. Schumann, J. B. Henry, L. Hoffmann, and L. Pfister (2007), Integration of SAR-derived river inundation areas, high-precision topographic data and a river flow model toward near real-time flood management, *Int. J. Appl. Earth Obs.*, *9*(3), 247–263.

McIntyre, N., and A. Al-Qurashi (2009), Performance of ten rainfall-runoff models applied to an arid catchment in Oman, *Environ. Modell. Software*, *24*, 726–738.

McIntyre, N., A. Al-Qurashi, and H. Wheater (2007), Regression analysis of rainfall-runoff data from an arid catchment in Oman, *Hydrol. Sci. J.*, *52*(6), 1103–1118.

McMillan, H., and M. Clark (2009), Rainfall-runoff model calibration using informal likelihood measures within a Markov chain Monte Carlo sampling scheme, *Water Resour. Res.*, *45*, W04418, doi:10.1029/2008WR007288.

Michaud, J., and S. Sorooshian (1994), Comparison of simple versus complex runoff models on a midsized semiarid watershed, *Water Resour. Res.*, *30*(3), 593–605.

Moran, M. S., et al. (2008), Preface to special section on fifty years of research and data collection: U.S. Department of Agriculture Walnut Gulch Experimental Watershed, *Water Resour. Res.*, *44*, W05S01, doi:10.1029/2007WR006083.

Morin, E., D. C. Goodrich, R. A. Maddox, X. G. Gao, H. V. Gupta, and S. Sorooshian (2006), Spatial patterns in thunderstorm rainfall events and their coupling with watershed hydrological response, *Adv. Water Resour.*, *29*(6), 843–860.

Morin, E., T. Grodek, O. Dahan, G. Benito, C. Kulls, Y. Jacoby, G. Van Langenhove, M. Seely, and Y. Enzel (2009), Flood routing and alluvial aquifer recharge along the ephemeral arid Kuiseb River, Namibia, *J. Hydrol.*, *368*, 262–275.

Mudd, S. M. (2006), Investigation of the hydrodynamics of flash floods in ephemeral channels: Scaling analysis and simulation using a shock-capturing flow model incorporating the effects of transmission losses, *J. Hydrol.*, *324*(1–4), 65–79.

Nichols, M. H., and C. Shipek (2006), Channel response to changes in runoff regime along the Walnut Gulch Channel, paper presented at Research Insights into Semi-arid Ecosystems Third Annual Symposium, Univ. of Ariz., Tucson, 7 Oct.

National Weather Service (2002), Advanced hydrologic prediction services concept of services and operations, report, NOAA, Nat. Weather Serv., Silver Spring, Md.

Parissopoulos, G. A., and H. S. Wheater (1991), Effects of Wadi flood hydrograph characteristics on infiltration, *J. Hydrol.*, *126*(3–4), 247–263.

Parsons, A. J., J. Wainwright, R. E. Brazier, and D. M. Powell (2006), Is sediment delivery a fallacy?, *Earth Surf. Processes Landforms*, *31*(10), 1325–1328.

Pelettier, J. D., and S. DeLong (2004), Oscillations in arid alluvial-channel geometry, *Geology*, *32*, 713–716.

Rawls, W. J., L. R. Ahuja, D. L. Brakensiek, and A. Shirmohammadi (1993), Infiltration and soil water movement, in *Handbook of Hydrology*, edited by D. R. Maidment, pp. 5.1–5.51, McGraw-Hill, New York.

Rayburg, S., M. Thoms, and M. Neave (2009), A comparison of digital elevation models generated from different data sources, *Geomorphology*, *106*, 261–270.

Refsgaard, J. C., J. P. van der Sluijs, J. Brown, and P. van der Keur (2006), A framework for dealing with uncertainty due to model structure error, *Adv. Water Resour.*, *29*, 1586–1597.

Renard, K. G., M. H. Nichols, D. A. Woolhiser, and H. B. Osborn (2008), A brief background on the U. S. Department of Agriculture Agricultural Research Service Walnut Gulch Experimental Watershed, *Water Resour. Res.*, *44*, W05S02, doi:10.1029/2006WR005691.

Seager, R., et al. (2007), Model projections of an imminent transition to a more arid climate in southwestern North America, *Science*, *316*(5828), 1181–1184.

Sharma, K. D., and J. S. R. Murthy (1995), Hydrologic routing of flow in arid ephemeral channels, *J. Hydraul. Eng.*, *121*(6), 466–471.

Smith, B. J., D. C. Goodrich, D. A. Woolhiser, and C. L. Unkrich (1995), KINEROS—A Kinematic runoff and erosion model, in *Computer Models of Watershed Hydrology*, edited by V. P. Singh, pp. 697–732, Water Resour. Publ., Highlands Ranch, Colo.

Wainwright, J., A. J. Parsons, E. N. Muller, R. E. Brazier, D. M. Powell, and B. Fenti (2008), A transport-distance approach to scaling erosion rates: 2. Sensitivity and evaluation of MAHLERAN, *Earth Surf. Processes Landforms*, *33*(6), 962–984.

Walters, M. O. (1990), Transmission losses in arid region, *J. Hydraul. Eng. ASCE*, *116*(1), 129–138.

Yatheendradas, S., T. Wagener, H. Gupta, C. Unkrich, D. Goodrich, M. Schaffner, and A. Stewart (2008), Understanding uncertainty in distributed flash flood forecasting for semiarid regions, *Water Resour. Res.*, *44*, W05S19, doi:10.1029/2007WR005940.

R. E. Brazier and A. P. Nicholas, Geography, College of Life and Environmental Sciences, University of Exeter, Rennes Dr., EX4 4RJ Exeter, UK.

C. J. Hutton, Centre for Water Systems, College of Engineering, Mathematics and Physical Sciences, University of Exeter, Harrison Building, North Park Road, EX4 4QF, Exeter, U.K. (c.j.hutton@ex.ac.uk)

M. Nearing, Southwest Watershed Research Center, United States Department of Agriculture, 2000 East Allen Rd., Tucson, AZ 85719, USA.